

Article

High-Mode Purity 1 μm Cylindrical Vector Beam All-Fiber Laser Based on a Symmetric Two-Mode Coupler

Boyi Yang^{1,2,3}, Siqi Pei^{1,2,3}, Tianyu Zhang^{1,2,3}, Yizhuo Zhang⁴, He Hao⁴, Kun Zhang⁵, Xuesheng Liu^{1,2,3,*}, Tian Lan^{1,2,3}, Anru Yan^{1,2,3}, Youqiang Liu^{1,2,3} and Zhiyong Wang^{1,2,3}

¹ Beijing Engineering Research Central of Laser Technology, Beijing University of Technology, Beijing 100124, China

² Key Laboratory of Trans-Scale Laser Manufacturing Technology, Beijing University of Technology, Ministry of Education, Beijing 100124, China

³ Institute of Advanced Technology on Semiconductor Optics & Electronics, Institute of Laser Engineering, Beijing University of Technology, Beijing 100124, China

⁴ AVIC Beijing Aeronautical Manufacturing Technology Research Institute, Beijing 100024, China

⁵ Science and Technology on Solid-State Laser Laboratory, No. 11 Research Institute of China Electronics Technology Group Corporation, Beijing 100015, China

* Correspondence: liuxuesheng@bjut.edu.cn; Tel.: +86-138-1043-5431

Abstract: Cylindrical vector beams (CVBs) are the product of polarization modulation of optical fields, and possess both unique focusing characteristics and excellent properties applicable to machining, imaging, communication and other fields. Mode selection couplers comprise a promising new method to realize the long-term stable output of cylindrical vector beam all-fiber lasers. Mode selection couplers have the advantages of a simple structure, high mode conversion efficiency and high mode purity. However, the production process of conventional asymmetric mode selection couplers is more complicated. Therefore, in this paper, a symmetric two-mode coupler with a 1 μm band is designed and fabricated using the finite element method, beam propagation method and fused pull-cone method, and a set of all-fiber passive mode-locked lasers based on symmetric dual-mode couplers are constructed. Finally, we obtain cylindrical vector beam outputs with central wavelengths of 1038.97 nm/1067.72 nm, a repetition rate of 8.78 MHz, pulse durations of 660 ps/656 ps, maximum average powers of 5.25 mW/5.2 mW, and the high mode purity of TM (transverse magnetic)₀₁ mode and TE (transverse electric)₀₁ mode is 97.18% and 97.07%, respectively.

Keywords: symmetric two-mode coupler; cylindrical vector beams; high mode purity; mode-locked



Citation: Yang, B.; Pei, S.; Zhang, T.; Zhang, Y.; Hao, H.; Zhang, K.; Liu, X.; Lan, T.; Yan, A.; Liu, Y.; et al. High-Mode Purity 1 μm Cylindrical Vector Beam All-Fiber Laser Based on a Symmetric Two-Mode Coupler. *Appl. Sci.* **2023**, *13*, 6490. <https://doi.org/10.3390/app13116490>

Academic Editor: Ju Han Lee

Received: 27 March 2023

Revised: 20 May 2023

Accepted: 22 May 2023

Published: 26 May 2023



Copyright: © 2023 by the authors. Licensee MDPI, Basel, Switzerland. This article is an open access article distributed under the terms and conditions of the Creative Commons Attribution (CC BY) license (<https://creativecommons.org/licenses/by/4.0/>).

1. Introduction

CVBs have axisymmetric intensity and polarization distribution, and under strong focusing conditions, a unique and strong local longitudinal electric field is formed in any plane parallel to the optical axis [1,2]. Relying on this feature, in terms of laser cutting, smaller and stronger light spots can be generated after CVB focusing; thus, the cutting depth-to-width ratio can be significantly improved using CVB cutting, and the cutting speed can be increased to 1.5–2 times that of conventional cutting [3,4]. CVB cutting has a wide range of applications in thick-plate cutting. In terms of laser drilling, CVB drilling can obtain straight holes with favorable height–width–depth ratios and a high punching rate [5,6]. Therefore, CVB processing is an effective scheme to improve processing quality and efficiency. In addition, under strong focusing conditions, CVB has a small focusing spot, and its application in high-resolution optical imaging system can greatly improve system resolution [7–9]. The TM₀₁ mode generates a large gradient and light field scattering force; therefore, it has a stronger trapping ability than Gaussian light, and can be used for particle trapping [10,11] and particle acceleration [12,13]. In the environment constituting strong scattering in water, CVB has a higher transmittance than traditional Gaussian light and can be used for wireless optical communication [14–16].

Initially, research related to CVBs has mainly focused on solid-state lasers. However, solid-state lasers have serious thermal effects and poor system reliability, coupled with the insertion of specially designed conical elements [17], birefringence elements [18], interference elements [19], sub-wavelength gratings [20], and other spatial devices, which seriously limit the capabilities of CVBs in practical applications. Compared with solid-state lasers, all-fiber lasers are convenient for thermal management and have a flexible structure, high beam quality, and high stability; therefore, all-fiber lasers are likely to become the main development direction for high-power CVBs. After nearly 10 years of development, the realization of mode conversion mainly includes bias-core coupling [21–24], long-period grating [25], special optical fibers [26–28], spatial Q-wave chips [29], mode selection couplers [30–33], etc., among which the use of mode selection couplers is the simplest way to achieve mode conversion and can obtain high mode purity, while offering low production costs, strong stability, and adaptability to complex engineering application environments.

To date, a number of institutions have carried out research on asymmetric structural mode selection couplers. In 2014, Ismaeel Rand et al. of the University of Southampton [30] made an asymmetric mode selection coupler, which realized the conversion of an LP_{01} (linear polarized) mode to an LP_{11} mode when the transmission wavelength was 1550 nm, with a coupling efficiency of 91%, a mode purity of 92%, and an insertion loss of 0.5 dB. In 2017, Hongdan Wan et al. of Nanjing University of Posts and Telecommunications [31] made an asymmetric mode selection coupler and built a figure-8-shaped mode-locked resonator, obtaining an LP_{11} mode output with a central wavelength of 1556.3 nm, and a pulse width of 17 ns, with a mode purity of 94.2% and an insertion loss of 0.65 dB. In 2018, Yiping Huang et al. of Shanghai University [32] fabricated an asymmetric mode selection coupler, and built a passive mode-locked fiber laser, obtaining an LP_{11} mode output with an average power of 75 mW, a coupling efficiency of 89%, and a central wavelength of 1043 nm. In 2018, Mao Dong et al. of Northwestern Polytechnical University [33] made a 1550 nm band asymmetric mode selection coupler, and built a ring-cavity passive mode-locked laser, which realized an LP_{11} mode output with pulse width adjustable from 39.2/31.9 ps to 5.6/5.2 ps. In 2019, Ya Shen et al. of Beijing Jiao Tong University [34] made an asymmetric mode selection coupler in the 1550 nm band and built a doped annular cavity fiber laser, and obtained an LP_{01} mode output with a central wavelength of 1550 nm and a mode purity of 94%. In 2019, Zhang Jiaojiao et al. of Nanjing University of Posts and Telecommunications [35] made an asymmetric mode selection coupler to obtain an LP_{11} mode output, and built a mode-locked laser to achieve an LP_{11} mode output with a pulse width of 629 ps and a mode purity of 94.5%.

Based on the coupling principle, we design and manufacture an all-fiber symmetrical two-mode coupler (STMC) in the 1 μm band for the first time that can achieve high-purity conversion from an LP_{01} mode to an LP_{11} mode. Then, we provide a feasible solution for CVB all-fiber lasers.

2. Materials and Methods

As shown in Figure 1, the STMC is made of two identical two-mode fibers (Corning SMF-28e, core/cladding = 8.2/125 μm , $n_{\text{core}} = 1.4637$, $n_{\text{cladding}} = 1.457$), and completes the excitation of the LP_{11} mode in the conical region and the output of the LP_{11} mode in the coupling region to realize the conversion of the LP_{01} mode to the LP_{11} mode.

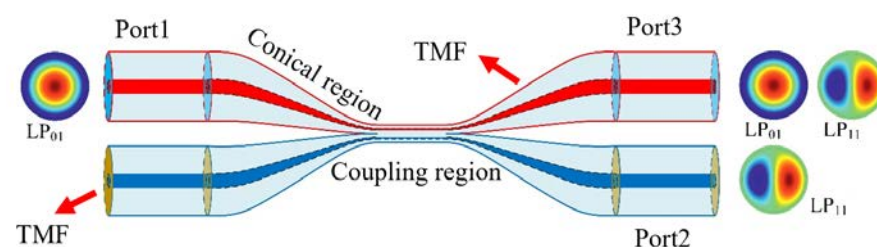


Figure 1. The structure and principle of STMC.

The coupling region working mechanism of the STMC conforms to mode-coupling theory, and the coupling equation is [36] as follows:

$$\frac{dA(z)}{dz} = jK_{21}B(z)e^{j(\beta_A - \beta_B)z} \tag{1}$$

$$\frac{dB(z)}{dz} = jK_{12}A(z)e^{j(\beta_B - \beta_A)z} \tag{2}$$

In the equation, $A(z)$ and $B(z)$ are the power distributions of the two modes along the axis; β is the propagation constant; z is the distance that light travels along the coupling region; and K is the coupling coefficient.

If light is incident only from the first two-mode fiber (TMF), the boundary conditions $A(0) = 1$ and $B(0) = 0$ are met. From this, Equation (2) is integrated:

$$B(L) = jK_{12} \int_0^L A(z)e^{j(\beta_B - \beta_A)z} dz \tag{3}$$

It can be seen that when the light transmission distance is L in the second FMF or TMF, a light wave field with power $B(L)$ is established. When $\beta_A - \beta_B \neq 0$, Equation (3) is equal to an effective value within the coupling distance L , that is, only if there are two modes or the same mode with similar propagation constants (equal effective refractive index) can a valid value be obtained, in which case effective coupling occurs.

In traditional mode selection couplers, direct coupling between LP_{01} and LP_{11} modes occurs, while in the STMC, taper pulling of the TMF can excite the LP_{11} mode in the fiber [37]; therefore, there is a coupling of two modes in the coupling region of the STMC, that is, the coupling between the two LP_{01} modes and the coupling between the two LP_{11} modes. By controlling the cone size of the TMF, the LP_{01} mode can be limited to the fiber core with minimal coupling to the other fiber, and the LP_{11} mode can be leaked into the cladding in order to be more coupled; specific size control is shown in the simulation analysis below.

We used the finite element method (FEM) to calculate the variation in the effective refractive index of LP_{01} and LP_{11} modes with the fiber diameter (cladding diameter) as in the SMF-28e fiber; the results are shown in Figure 2. According to the principle of total internal reflection, the condition under which the mode is tethered to the core in the SMF-28e fiber is $1.457 < n_{eff} < 1.4637$. When the effective refractive index of the mode is less than 1.457, the mode leaks into the cladding.

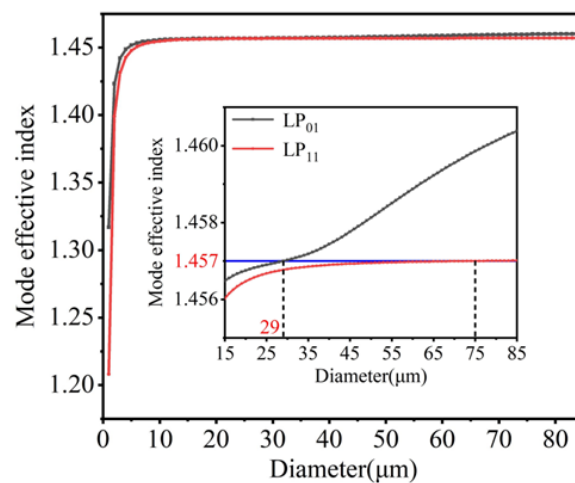


Figure 2. The change curve of effective refractive index with fiber diameter.

As shown in Figure 2, (The illustration in Figure 2 is a part of the figure in Figure 2. Its actual meaning is the distribution of mode LP_{01} and mode LP_{11} when the fiber diameter is

15–85 μm , the blue line is the cladding index of TMF.) by controlling the tensile diameter of the fiber, the LP_{01} mode in the TMF can be bound in the core, and the LP_{11} mode leaks into the cladding, so that the LP_{01} mode is separated from the LP_{11} mode. According to the simulation results, when the fiber diameter is 75 μm , the effective refractive index of the LP_{11} mode in the TMF is 1.457; at this time, the LP_{11} mode begins to leak into the cladding, and LP_{11} mode coupling begins to occur in the coupling region of the STMC, while the effective refractive index of the LP_{01} mode is $1.457 < n_{\text{eff}} < 1.4637$. At this time, the LP_{01} mode is bound to the core for transmission; therefore, the coupling of the LP_{01} mode occurs only to a minor degree in the coupling region of the STMC. Similarly, when the diameter of the fiber is 29 μm , the effective refractive index of the LP_{01} mode in the TMF is 1.457, at which time the LP_{01} mode begins to leak into the cladding, and LP_{01} mode coupling begins to occur in the coupling region of the STMC. When this happens, the purity of the LP_{11} mode at port2 decreases. Therefore, in order to minimize LP_{01} mode coupling in the coupling region and improve the output purity of the LP_{11} mode, the diameter of the fiber cone should be between 29 μm and 75 μm .

We used the beam propagation method (BPM) to creatively establish a conical three-dimensional waveguide model of the STMC. According to the cone simulation results shown in Figure 3, as the diameter of the TMF gradually decreases, the LP_{11} mode gradually leaks from the core to the cladding for transmission. When the fiber diameter is stretched to 30 μm and 31 μm , the LP_{11} mode has completely leaked out of the core and, at this time, the LP_{01} mode is still bound in the core, only minimally leaking into the cladding. It can be seen that when the TMF fiber diameter is stretched to 30 μm and 31 μm , the separation of LP_{01} and LP_{11} modes can be effectively realized.

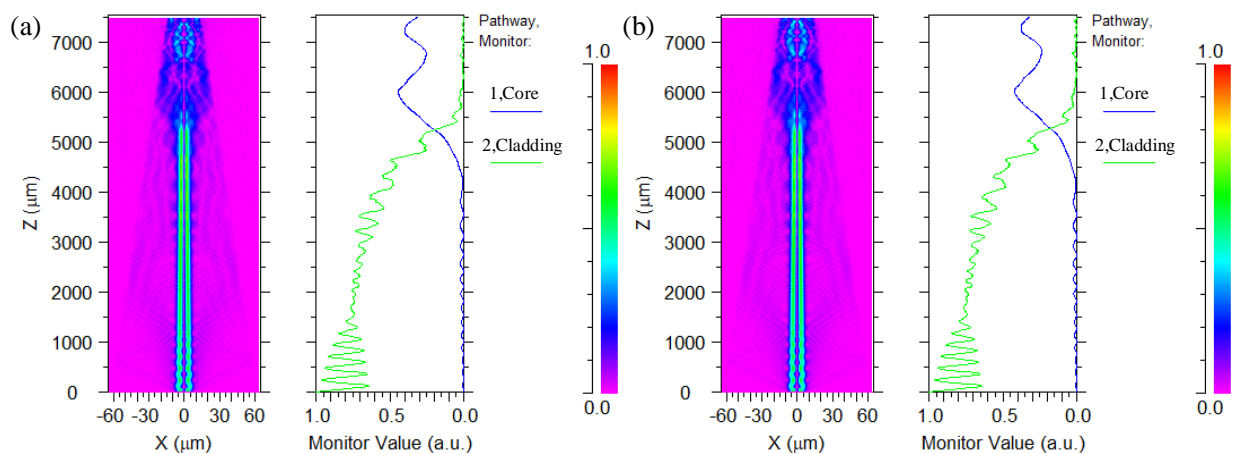


Figure 3. LP_{11} mode longitudinal energy flow simulation during TMF cone pulling, diameter (μm) after TMF cone pulling: (a) 30 μm ; (b) 31 μm .

Referring to the simulation results of the cone region, we used the BPM to establish a three-dimensional waveguide model of the coupling region of the STMC, and the simulation results are shown in Figure 4.

According to the simulation results of the energy flow shown in Figure 4, regardless of whether the stretch is 30 μm or 31 μm , the energy exchange between the two fibers shows a periodic change law, and when the coupling length is chosen properly, the LP_{11} mode in the first fiber can be almost completely coupled to the other fiber. In this paper, it is said that the optimal coupling length is the shortest distance transmitted when the LP_{11} mode energy is coupled from the first fiber to the second fiber maximally. According to the simulation results shown in the figure, when the diameter of SMF-28e's coupling zone is 30 μm , the optimal coupling length is about 4.5 cm and 5.5 cm for the first and second fibers, respectively. Finally, based on the above simulation results of the STMC, we used the fused tapered method to complete the STMC. The physical picture of the STMC is shown in Figure 5.

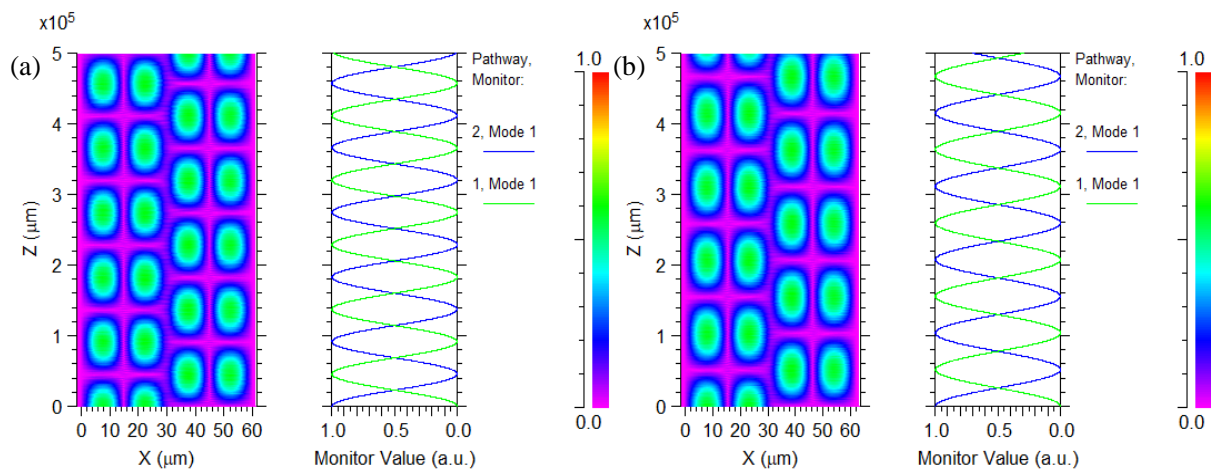


Figure 4. Energy flow simulation results of STMC, TMF diameter (μm): (a) 30; (b) 31.

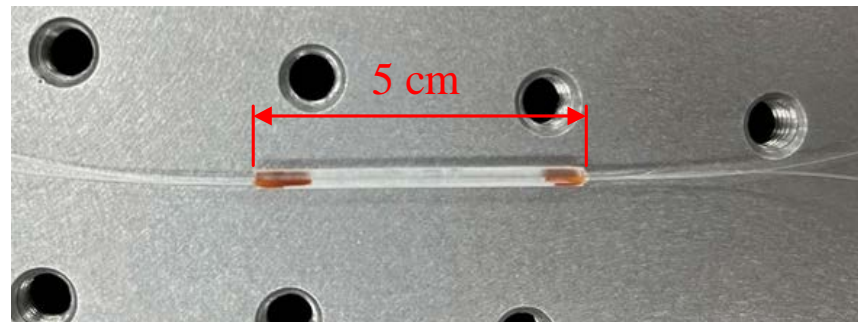


Figure 5. STMC physical picture.

3. Nonlinear Polarization Rotation Principle

The structure of nonlinear polarization rotation principle (NPR) mode clamping is shown in Figure 6, including two polarization controllers (PC) and a polarization-dependent isolator (PDI). PC1 is equivalent to a $1/2$ wave plate, PC2 is equivalent to a $1/4$ wave plate, and the PDI has three functions, namely as an isolator, polarizer, and polarization detector. Its working principle is as follows: light after PDI is converted into linear polarized light and after PC2, into elliptically polarized light. Elliptical polarized light can be regarded as the superposition of two orthogonal linear polarized lights; the light intensity of these two decomposed lights is different. Due to the influence of nonlinear effects, different intensities of light produce different nonlinear phase shifts in the transmission of optical fibers. When the light pulse returns to PC1, the polarization direction of the optical pulse is changed by adjusting PC1, so that the part with higher light intensity near the center of the light pulse passes through with low loss, and the part with weak light intensity near the edge of the light pulse is filtered; thus, the light pulse is continuously narrowed in multiple cycles. Finally, a stable mode-locked pulse laser output is obtained.

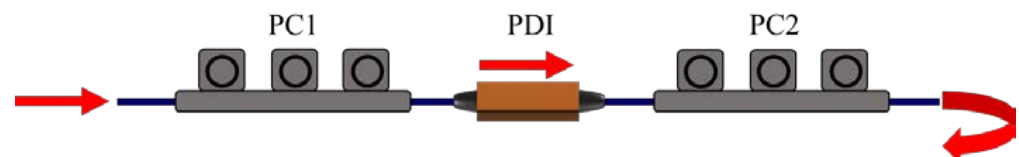


Figure 6. Schematic diagram of the NPR structure.

4. Experimental Setup

We use NPR technology to carry out CVB mode-locked laser research, as shown in Figure 7. The current laser cavity comprises a 980/1064 nm wavelength division multiplexing (WDM) and a 2 m ytterbium-doped fiber (YDF, Nufern SM-YSF-HI-HP) pumped by

a 976 nm laser diode (LD). The absorption coefficient of the YDF at 975 nm is 250 dB/m and the polarization-dependent isolator (PDI) and the polarization controller (PC) together form an NPR mode-locked module. A 7 m long single-mode fiber (SMF, Nufern 1060XP) was used for nonlinear and dispersion management; the length of the current laser cavity is about 23 m. Using a 45/55 single-mode fiber coupler as the LP₀₁ mode output of the current laser cavity, because YDF and SMF have positive dispersion in the 1 μm band, the entire laser works in the full positive dispersion region. The LP₀₁ mode is converted to the LP₁₁ mode by the STMC with the output of the pulse laser, which is received by the CCD after attenuation, and the output of TM₀₁ and TE₀₁ modes can be realized by adjusting PC3.

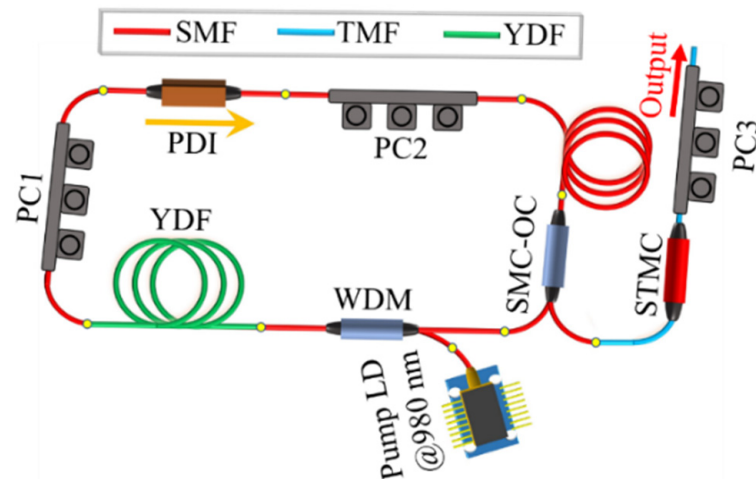


Figure 7. CVB all-fiber mode-locked experimental setup.

5. Results and Discussion

When the pump power is greater than 300 mW, by adjusting PC1 and PC2, the mode-locked laser output with two central wavelengths of 1038.97 nm and 1067.72 nm can be realized.

When the central wavelength is 1038.97 nm, the output of the mode-locked CVB fiber laser is as shown in Figure 8. Figure 8a shows the output spectrum, which yields a 3 dB linewidth of 2.99 nm. Figure 8b is a pulse train, wherein the pulse interval is 113.8 ns and the repetition frequency is 8.78 MHz, which is consistent with the theoretical calculation value of 23 m cavity length, referring to the formula $f = c/nL$. Figure 8c is the corresponding single pulse; the single pulse has Gaussian distribution, and the pulse width is 660 ps. Figure 8d is the change curve of laser output power with pump power. It can be seen that the average output power of the laser is linearly positively correlated with the pump power. This experiment is limited by cavity loss and pump power; the maximum average output power of the LP₁₁ mode is 5.56 mW. When PC3 is properly adjusted, we obtain CVBs with a maximum output average power of 5.2 mW. This is illustrated in the mode intensity distribution of the laser output.

When the central wavelength is 1067.72 nm, the output of the mode-locked CVB fiber laser is as shown in Figure 9. The laser output pulse train and repetition rate are consistent with the output results when the central wavelength is 1038.97 nm; the pulse width of the single pulse is 656 ps. Figure 9d is the change curve of laser output power with pump power. We can see that the average output power of the laser and the pump power also have a linear positive correlation, also limited by cavity loss and pump power; the maximum average output power of the LP₁₁ mode is 5.5 mW and the maximum output average power of CVBs is 5.2 mW. This is illustrated in the mode intensity distribution of the laser output.

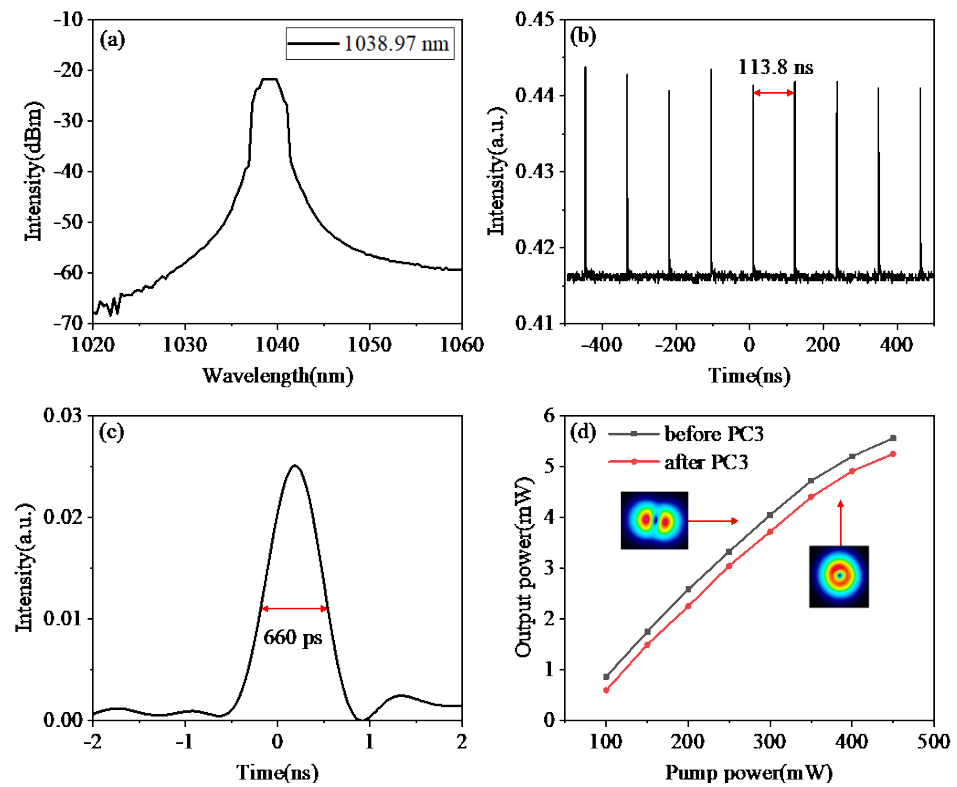


Figure 8. The output characteristics of mode-locked fiber laser at a pump power of 300 mW (central wavelength: 1038.97 nm): (a) spectrum; (b) output pulse train; (c) single pulse; (d) the change curve of output power with pump power.

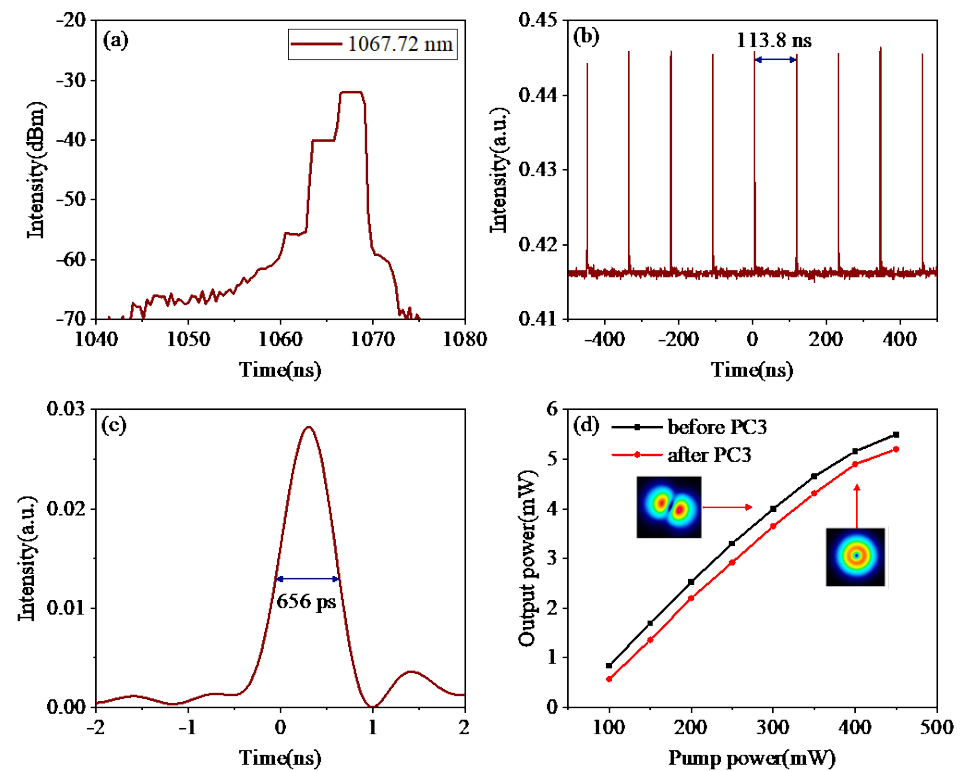


Figure 9. The output characteristics of mode-locked fiber laser at a pump power of 300 mW (central wavelength: 1067.72 nm): (a) spectrum; (b) output pulse train; (c) single pulse; (d) the change curve of output power with pump power.

The relatively low CVB output power is determined by the design and production process of the STMC itself. The specific reason is that in order to obtain a high-purity LP₁₁ mode during the production process of the STMC, the LP₁₁ mode should leak into the cladding as much as possible, while the LP₀₁ mode should be restricted in the fiber core. Thus, the separation of LP₀₁ and LP₁₁ modes is maximized, which requires a specific fiber diameter range in the coupling region, thus limiting the CVB output power of the STMC. According to the simulation results above, when the diameter of the STMC-coupling region is larger than 75 μm , both LP₀₁ and LP₁₁ modes are bound in the fiber core and are not coupled to the second TMF. When the diameter of the STMC-coupling region was 29–75 μm , the evanescent field of the LP₁₁ mode was not strong, while the LP₀₁ mode was still bound in the fiber core, and the optical power coupling was very weak, which resulted in low optical power coupling efficiency and CVB output power. When the diameter of the fiber in the coupling region is further reduced to less than 29 μm , the LP₀₁ mode begins to be coupled to the second TMF. At this time, the output power is increased, but the increased power is the power of the LP₀₁ mode, and the purity of the LP₁₁ mode is reduced. Although the output power is low, the production process of the STMC is simple and the production cost is low, which eliminates the complicated pre-taper process used in the production of mode selection couplers. In addition, the commercial Corning SMF-28e is used to design and manufacture the STMC, so as to avoid the complicated design and production process of 1 μm band TMFs, which has great engineering application potential.

By adjusting PC3, CVBs with a torus intensity pattern distribution can be obtained, and TM₀₁ and TE₀₁ modes can be distinguished by rotating the polarizer. The mode intensity distribution of TM₀₁ and TE₀₁ modes was obtained using a CCD camera (DataRay, WinCamD-LCM). The results are shown in Figure 10. The purity of TM₀₁ and TE₀₁ modes was measured to be 97.18% and 97.07%, respectively. We can conclude that the STMC achieves a high-quality TM₀₁ or TE₀₁ mode output, and the output mode is tunable.

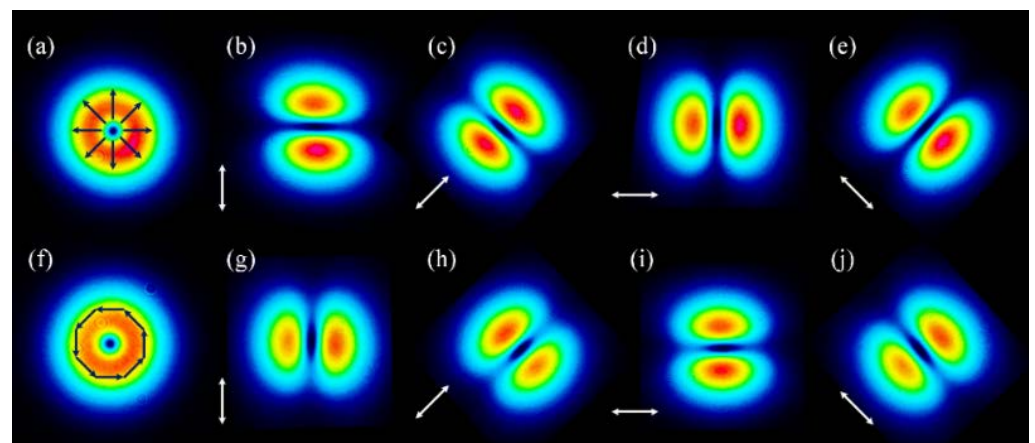


Figure 10. (a) TM₀₁ mode; (b–e) mode distribution after TM₀₁ mode passes through polarizers in different directions; (f) TE₀₁ mode; (g–j) mode distribution of the TE₀₁ mode passes through polarizers in different directions.

6. Conclusions

In this paper, an all-fiber symmetrical two-mode coupler with a 1 μm band that can realize the conversion of the LP₀₁ mode to the LP₁₁ mode with high purity is designed and produced, and a feasible solution for CVB all-fiber lasers is provided. Finally, we obtain a CVB output with working central wavelengths of 1038.97 nm/1067.72 nm, a repetition of 8.78 MHz, pulse widths of 660 ps/656 ps, and maximum output average powers of 5.25 mW/5.2 mW. By adjusting PC3, we can obtain TM₀₁ and TE₀₁ modes with mode purity values of 97.18%/97.07%, respectively. To our knowledge, this is the first time that a symmetrical two-mode coupler has been obtained using two identical commercial Corning SMF-28e fibers, and the highest mode purity 1 μm all-fiber CVB output was

obtained, which minimizes the manufacturing process of mode selection couplers and reduces manufacturing costs. In future work, the process of taper excitation of the LP₁₁ mode should be simulated and analyzed to investigate the factors affecting the mode conversion efficiency of the STMC, and special optical fibers should be designed to improve the mode conversion efficiency of the STMC.

Author Contributions: Conceptualization, B.Y. and X.L.; methodology, B.Y., X.L., Y.L. and Z.W.; formal analysis, H.H., K.Z. and Y.Z.; investigation, S.P. and T.Z.; data curation, B.Y.; writing—original draft preparation, B.Y.; writing—review and editing, B.Y.; supervision, T.L. and A.Y.; project administration, X.L.; funding acquisition, X.L. All authors have read and agreed to the published version of the manuscript.

Funding: This research was funded by the Beijing Municipal Natural Science Foundation(1212009); the Basic Scientific Research(JCKY2021110B175); the Rapid Support Programme(80914020105); and the Open Fund for Key Laboratory of Solid-State Laser Technology.

Institutional Review Board Statement: Not applicable.

Informed Consent Statement: Not applicable.

Data Availability Statement: Data underlying the results presented in this paper are not publicly available at this time but may be obtained from the authors upon reasonable request.

Conflicts of Interest: The authors declare no conflict of interest.

References

1. Youngworth, K.; Brown, T. Focusing of High Numerical Aperture Cylindrical-Vector Beams. *Opt. Express* **2000**, *7*, 77–87. [[CrossRef](#)] [[PubMed](#)]
2. Zhan, Q.W.; Leger, J.R. Focus shaping using cylindrical vector beams. *Opt. Express* **2002**, *10*, 324–331. [[CrossRef](#)] [[PubMed](#)]
3. Niziev, V.G.; Nesterov, A.V. Influence of beam polarization on laser cutting efficiency. *J. Phys. D Appl. Phys.* **1999**, *32*, 1455–1461. [[CrossRef](#)]
4. Weber, R.; Michalowski, A.; Abdou-Ahmed, M.; Onuseit, V.; Rominger, V.; Kraus, M.; Graf, T. Effects of Radial and Tangential Polarization in Laser Material Processing. *Phys. Procedia* **2011**, *12*, 21–30. [[CrossRef](#)]
5. Kraus, M.; Ahmed, M.A.; Michalowski, A.; Voss, A.; Weber, R.; Graf, T. Microdrilling in steel using ultrashort pulsed laser beams with radial and azimuthal polarization. *Opt. Express* **2010**, *18*, 22305–22313. [[CrossRef](#)]
6. Matsusaka, S.; Kozawa, Y.; Sato, S. Micro-Hole Drilling by Tightly Focused Vector Beams. *Opt. Lett.* **2018**, *43*, 1542–1545. [[CrossRef](#)]
7. Biss, D.P.; Brown, T.G. Polarization-vortex-driven second-harmonic generation. *Opt. Lett.* **2003**, *28*, 923–925. [[CrossRef](#)]
8. Carrasco, S.; Saleh, B.E.A.; Teich, M.C.; Fourkas, J.T. Second- and third-harmonic generation with vector Gaussian beams. *J. Opt. Soc. Am. B* **2006**, *23*, 2134–2141. [[CrossRef](#)]
9. Kozawa, Y.; Matsunaga, D.; Sato, S. Superresolution imaging via superoscillation focusing of a radially polarized beam. *Optica* **2018**, *5*, 86–92. [[CrossRef](#)]
10. Zhan, Q.W. Trapping metallic Rayleigh particles with radial polarization. *Opt. Express* **2004**, *12*, 3377–3382. [[CrossRef](#)]
11. Zhan, Q.W. Radiation Forces on a Dielectric Sphere Produced by Highly Focused Cylindrical Vector Beams. *J. Opt. A Pure Appl. Opt.* **2003**, *5*, 229–232. [[CrossRef](#)]
12. Modena, A.; Najmudin, Z.; Dangor, A.E.; Clayton, C.E.; Marsh, K.A.; Joshi, C.; Malka, V.; Darrow, C.B.; Danson, C.; Neely, D.; et al. Electron acceleration from the breaking of relativistic plasma-waves. *Nature* **1995**, *377*, 606–608. [[CrossRef](#)]
13. Malka, V.; Fritzler, S.; Lefebvre, E.; Aleanard, M.-M.; Burgy, F.; Chambaret, J.-P.; Chemin, J.-F.; Krushelnick, K.; Malka, G.; Mangles, S.P.D.; et al. Electron Acceleration by a Wake Field Forced by an Intense Ultrashort Laser Pulse. *Science* **2002**, *298*, 1596–1600. [[CrossRef](#)]
14. Baghdady, J.; Miller, K.; Morgan, K.; Byrd, M.; Osler, S.; Ragusa, R.; Li, W.; Cochenour, B.M.; Johnson, E.G. Multi-gigabit/s underwater optical communication link using orbital angular momentum multiplexing. *Opt. Express* **2016**, *24*, 9794–9805. [[CrossRef](#)] [[PubMed](#)]
15. Wang, A.-D.; Zhu, L.; Zhao, Y.-F.; Li, S.-H.; Lv, W.-C.; Xu, J.; Wang, J. Adaptive water-air-water data information transfer using orbital angular momentum. *Opt. Express* **2018**, *26*, 8669–8678. [[CrossRef](#)]
16. Karahroudi, M.K.; Moosavi, S.A.; Mobashery, A.; Parmoon, B.; Saghaififar, H. Performance evaluation of perfect optical vortices transmission in an underwater optical communication system: Publisher’s note. *Appl. Opt.* **2018**, *57*, 9148–9154. [[CrossRef](#)] [[PubMed](#)]
17. Li, J.-L.; Ueda, K.-I.; Musha, M.; Shirakawa, A.; Zhong, L.-X. Generation of radially polarized mode in Yb fiber laser by using a dual conical prism. *Opt. Lett.* **2006**, *31*, 2969–2971. [[CrossRef](#)]

18. Thirugnanasambandam, M.P.; Senatsky, Y.; Ueda, K.-I. Generation of radially and azimuthally polarized beams in Yb:YAG laser with intra-cavity lens and birefringent crystal. *Opt. Express*. **2011**, *19*, 1905–1914. [[CrossRef](#)]
19. Niziev, V.G.; Chang, R.S.; Nesterov, A.V. Generation of inhomogeneously polarized laser beams by use of a Sagnac interferometer. *Appl. Opt.* **2006**, *45*, 8393–8399. [[CrossRef](#)]
20. Lin, D.; Xia, K.; Li, J.; Li, R.; Ueda, K.-I.; Li, G.; Li, X. Efficient, high-power, and radially polarized fiber laser. *Opt. Lett.* **2010**, *35*, 2290. [[CrossRef](#)]
21. Grosjean, T.; Courjon, D.; Spajer, M. An all-fiber device for generating radially and other polarized light beams. *Opt. Commun.* **2002**, *203*, 1–5. [[CrossRef](#)]
22. Lin, D.; Xia, K.; Li, J.; Li, R.; Ueda, K.-I.; Li, G.; Li, X. An all-fiber laser generating cylindrical vector beam. *Opt. Express* **2010**, *18*, 10834–10838.
23. Sun, B.; Wang, A.; Gu, C.; Chen, G.; Xu, L.; Chung, D.; Zhan, Q. Mode-locked all-fiber laser producing radially polarized rectangular pulses. *Opt. Lett.* **2015**, *40*, 1691–1694. [[CrossRef](#)]
24. Zhou, Y.; Wang, A.; Gu, C.; Sun, B.; Xu, L.; Li, F.; Chung, D.; Zhan, Q. Actively mode-locked all fiber laser with cylindrical vector beam output. *Opt. Lett.* **2016**, *41*, 548–550. [[CrossRef](#)] [[PubMed](#)]
25. Liu, T.; Chen, S.; Qi, X.; Hou, J. High-power transverse-mode-switchable all-fiber picosecond MOPA. *Opt. Express* **2016**, *24*, 27821–27827. [[CrossRef](#)]
26. Li, J.L.; Wang, C.C.; Wang, W.Q. Generation of an azimuthally polarized beam with a metallic ring core fiber. *Appl. Opt.* **2013**, *52*, 7759–7768. [[CrossRef](#)]
27. Li, H.; Yan, K.; Zhang, Y.; Gu, C.; Yao, P.; Xu, L.; Zhang, R.; Su, J.; Chen, W.; Zhu, Y.; et al. Low-threshold high-efficiency all-fiber laser generating cylindrical vector beams operated in LP₁₁ mode throughout the entire cavity. *Appl. Phys. Express* **2018**, *11*, 122502. [[CrossRef](#)]
28. Zhang, Y.; Li, H.; Dai, C.; Xu, L.; Gu, C.; Chen, W.; Zhu, Y.; Yao, P.; Zhan, Q. All-fiber high-order mode laser using a metal-clad transverse mode filter. *Opt. Express* **2018**, *26*, 29679–29686. [[CrossRef](#)]
29. Lin, D.; Baktash, N.; Alam, S.-U.; Richardson, D.J. 106 W, picosecond Yb-doped fiber MOPA system with a radially polarized output beam. *Opt. Lett.* **2018**, *43*, 4957–4960.
30. Ismaeel, R.; Lee, T.; Oduro, B.; Jung, Y.; Brambilla, G. All-fiber fused directional coupler for highly efficient spatial mode conversion. *Opt. Express* **2014**, *22*, 11610–11619. [[CrossRef](#)]
31. Wan, H.; Wang, J.; Zhang, Z.; Cai, Y.; Sun, B.; Zhan, L. High efficiency mode-locked, cylindrical vector beam fiber laser based on a mode selective coupler. *Opt. Express* **2017**, *25*, 11444–11451. [[CrossRef](#)] [[PubMed](#)]
32. Huang, Y.; Shi, F.; Wang, T.; Liu, X.; Zeng, X.; Pang, F.; Wang, T.; Zhou, P. High-order mode Yb-doped fiber lasers based on mode-selective couplers. *Opt. Express* **2018**, *26*, 19171–19181. [[CrossRef](#)]
33. Mao, D.; He, Z.; Lu, H.; Li, M.; Zhang, W.; Cui, X.; Jiang, B.; Zhao, J. All-fiber radially/azimuthally polarized lasers based on mode coupling of tapered fibers. *Opt. Lett.* **2018**, *43*, 1590–1593. [[CrossRef](#)] [[PubMed](#)]
34. Shen, Y.; Yang, Y.; Jiang, Y.; Yao, S.; Jian, S.X.S. Radially polarized cylindrical vector beam generation in all-fiber narrow linewidth single-longitudinal-mode laser. *Laser Phys. Lett.* **2019**, *16*, 055101. [[CrossRef](#)]
35. Zhang, J.; Zhang, Z.; Xu, Y.; Wan, H.; Wang, J.; Zhang, L. Dissipative soliton resonance Ytterbium-doped fiber laser with cylindrical vector beam generation. *Opt. Laser Technol.* **2019**, *113*, 234–238. [[CrossRef](#)]
36. Snyder, A.W. Radiation on Losses Due to Variations of Radius Dielectric or Optical Fibers. *Microw. Theory Tech. IEEE Trans.* **1970**, *18*, 608–615. [[CrossRef](#)]
37. Sun, B.; Fang, F.; Zhang, Z.; Xu, J.; Zhang, L. High-sensitivity and low-temperature magnetic field sensor based on tapered two-mode fiber interference. *Opt. Lett.* **2018**, *43*, 1311–1314. [[CrossRef](#)]

Disclaimer/Publisher’s Note: The statements, opinions and data contained in all publications are solely those of the individual author(s) and contributor(s) and not of MDPI and/or the editor(s). MDPI and/or the editor(s) disclaim responsibility for any injury to people or property resulting from any ideas, methods, instructions or products referred to in the content.